Collective Motion From Consensus With Cartesian Coordinate Coupling

Wei Ren, *Member, IEEE*

***Abstract*—Collective motions including rendezvous, circular patterns, and logarithmic spiral patterns can be achieved by introducing Cartesian coordinate coupling to existing consensus algorithms. We study the collective motions of a team of vehicles in 3-D by introducing a rotation matrix to an existing consensus algorithm for double-integrator dynamics. It is shown that the network topology, the damping gain, and the value of the Euler angle all affect the resulting collective motions. We show that when the nonsymmetric Laplacian matrix has certain properties, the damping gain is above a certain bound, and the Euler angle is below, equal, or above a critical value, the vehicles will eventually rendezvous, move on circular orbits, or follow logarithmic spiral curves lying on a plane perpendicular to the Euler axis. In particular, when the vehicles eventually move on circular orbits, the relative radii of the orbits (respectively, the relative phases of the vehicles on their orbits) are equal to the relative magnitudes (respectively, the relative phases) of the components of a right eigenvector associated with a critical eigenvalue of the nonsymmetric Laplacian matrix. Simulation results are presented to demonstrate the theoretical results.**

***Index Terms*—Collective motion, consensus, cooperative control, distributed algorithms, multi-vehicle systems.**

I. Introduction

Coordination of robotic networks has received significant attention in recent years due to its potential impact in numerous civilian, homeland security, and military applications. Consensus plays an important role in achieving distributed coordination. The basic idea of consensus is that a team of vehicles reaches an agreement on a common value by negotiating with their neighbors. Consensus algorithms are studied for both single-integrator kinematics [1]–[3] and double-integrator dynamics [4]–[9], to name a few.

Related to consensus is the cyclic pursuit strategy, where each vehicle pursues only one other vehicle with the network topology forming a unidirectional ring. Cyclic pursuit is studied for single-integrator kinematics in [10], [11] while for wheeled vehicles subject to nonholonomic constraints in [12]. Ref. [13] generalizes the cyclic pursuit strategy by letting each vehicle pursue one other vehicle along the line of sight rotated by a common offset angle. It is shown that depending on the common offset angle, the vehicles can achieve different symmetric formations, namely, convergence to a single point, a circle, or a logarithmic spiral pattern. Other researchers also study symmetric formations by adopting models based on the Frenet-Serret equations of motion [14] or by exploring the connections between phase models of coupled oscillators and kinematic models of self-propelled particle groups [15].

While the strategy proposed in [13] generates interesting symmetric formation patterns, there are limitations. First, the results in [13] are limited to 2-D. However, for applications involving unmanned aerial vehicles, it will be more natural to study motions in 3-D. Second, the results in [13] primarily focus on single-integrator kinematics. While an extension to double-integrator dynamics is proposed to deal with a formation control problem, the extension relies not only on relative positions but also on relative velocities between neighbors. However, the requirement for the knowledge of relative velocities might be too restrictive for some applications. Third, the results in [13] rely on a unidirectional ring topology and the resulting circular and logarithmic spiral patterns are evenly spaced. However, for a team consisting of heterogenous vehicles with different sensing/communciation capabilities, it might not always be desirable that the vehicles are evenly spaced and move along the same orbit with an identical radius. It will also be interesting to study the motions resulting from a general (not necessarily unidirectional ring) network topology. To address these limitations, the strategy proposed in [13] needs to be extended.

In this note, we extend the results in [13] threefold, namely, i) extension from 2-D to 3-D, ii) extension from single-integrator kinematics to double-integrator dynamics without the knowledge of relative velocities, and iii) extension from a unidirectional ring topology to a general network topology to generate possibly non-evenly-spaced circular and logarithmic spiral patterns on concentric orbits with possibly nonidentical radii. In particular, we introduce Cartesian coordinate coupling to an existing consensus algorithm for double-integrator dynamics through a rotation matrix in 3-D, analyze the convergence properties, and quantitatively characterize the resulting collective motions in 3-D, namely, convergence to a point, circular patterns with concentric orbits, and logarithmic spiral curves lying on a plane perpendicular to the Euler axis, over a general network topology. The resulting collective motions are expected to have applications in rendezvous, persistent surveillance, and coverage control with teams of heterogeneous vehicles. It is shown that the network topology, the damping gain, and the value of the Euler angle all affect the resulting collective motions. Our analysis relies on algebraic graph theory, matrix theory, and properties of the Kronecker product. In particular, we will show that the convergence result in [13] is a special case of the results in this note and the convergence result in [13] can be recovered by exploiting the properties of circulant matrices and the Kronecker product. A preliminary version of the work has appeared in [16].

II. Background and Preliminaries

A. Graph Theory Notions

It is natural to model interaction among vehicles by directed graphs. Suppose that a team consists of n vehicles. A weighted directed graph $\mathcal{G}$ consists of a node set $\mathcal{V} = \{1, \ldots, n\}$, an edge set $\mathcal{E} \subseteq \mathcal{V} \times \mathcal{V}$, and a weighted adjacency matrix $\mathcal{A} = [a_{ij}] \in \mathbb{R}^{n \times n}$. An edge (i, j) denotes that vehicle j can obtain information from vehicle i, but not necessarily vice versa. Weighted adjacency matrix $\mathcal{A}$ associated with $\mathcal{G}$ is defined such that a_{ij} is a positive weight if $(j, i) \in \mathcal{E}$, while $a_{ij} = 0$ if $(j, i) \notin \mathcal{E}$. A directed path is a sequence of edges in a directed graph of the form $(i_1, i_2), (i_2, i_3), \ldots$, where $i_j \in \mathcal{V}$. A directed graph has a directed spanning tree if there exists at least one node having a directed path to all other nodes. Let nonsymmetric Laplacian matrix $\mathcal{L} = [\ell_{ij}] \in \mathbb{R}^{n \times n}$ associated with $\mathcal{A}$ be defined as $\ell_{ii} = \sum_{j=1, j \neq i}^{n} a_{ij}$ and $\ell_{ij} = -a_{ij}$, $i \neq j$ [17].

B. Existing Consensus Algorithm for Double-Integrator Dynamics

Consider vehicles with double-integrator dynamics given by

$$\dot{r}_i = v_i, \qquad \dot{v}_i = u_i, \quad i = 1, \ldots, n \tag{1}$$

Manuscript received March 27, 2008; revised October 04, 2008 and January 14, 2009. First published May 27, 2009; current version published June 10, 2009. This work was supported by a National Science Foundation CAREER Award (ECCS-0748287). Recommended by Associate Editor M. Egerstedt.

The author is with the Electrical and Computer Engineering Department, Utah State University, Logan, UT 84322 USA (e-mail: wren@engineering.usu.edu).

Color versions of one or more of the figures in this technical note are available online at http://ieeexplore.ieee.org

Digital Object Identifier 10.1109/TAC.2009.2015544

0018-9286/$25.00 © 2009 IEEE

Authorized licensed use limited to: Utah State University. Downloaded on June 15, 2009 at 15:55 from IEEE Xplore. Restrictions apply.

where $r_i \in \mathbb{R}^m$ and $v_i \in \mathbb{R}^m$ are, respectively, the position and velocity of the ith vehicle, and $u_i \in \mathbb{R}^m$ is the control input. A consensus algorithm for (1) is studied in [9], [18] as

$$u_i = -\sum_{j=1}^{n} a_{ij}(r_i - r_j) - \alpha v_i, \quad i = 1, \ldots, n \tag{2}$$

where a_{ij} is the (i,j)th entry of weighted adjacency matrix $\mathcal{A}$ associated with weighted directed graph $\mathcal{G}$, and α is a positive damping gain. Consensus is reached for (1) using (2) if for all $r_i(0)$ and $v_i(0)$, $r_i(t) \to r_j(t)$ and $v_i(t) \to 0$ as $t \to \infty$.

III. Consensus With Cartesian Coordinate Coupling

In this section, we consider a consensus algorithm for double-integrator dynamics (1) with Cartesian coordinate coupling as

$$u_i = -\sum_{j=1}^{n} a_{ij} C(r_i - r_j) - \alpha v_i, \quad i = 1, \ldots, n \tag{3}$$

where a_{ij} and α are defined as in (2), and $C \in \mathbb{R}^{m \times m}$ denotes a Cartesian coordinate coupling matrix. We assume that all vehicles know C and α *a priori* and the vehicles' positions and velocities are represented in a common reference frame. Note that (2) corresponds to the case where $C = I_m$, where I_m denotes the $m \times m$ identity matrix. That is, using (2), the components of r_i (i.e., the Cartesian coordinates of vehicle i) can be decoupled while using (3) the components of r_i are coupled.

A. Convergence Result

In this subsection, we analyze the convergence properties of (3). We focus on the case where C is a rotation matrix while a similar analysis can be extended to the case where C is a general matrix. Before moving on, we need the following lemmas and definition:

Lemma 3.1: Let $U \in \mathbb{R}^{p \times p}$, $V \in \mathbb{R}^{q \times q}$, $X \in \mathbb{R}^{p \times p}$, and $Y \in \mathbb{R}^{q \times q}$. Then $(U \otimes V)(X \otimes Y) = UX \otimes VY$, where $\otimes$ denotes the Kronecker product. Let $A \in \mathbb{R}^{p \times p}$ have eigenvalues β_i with associated eigenvectors $f_i \in \mathbb{C}^p$, $i = 1, \ldots, p$, and let $B \in \mathbb{R}^{q \times q}$ have eigenvalues ρ_j with associated eigenvectors $g_j \in \mathbb{C}^q$, $j = 1, \ldots, q$. Then the pq eigenvalues of $A \otimes B$ are $\beta_i \rho_j$ with associated eigenvectors $f_i \otimes g_j$, $i = 1, \ldots, p$, $j = 1, \ldots, q$.

Lemma 3.2: [3] Let $\mathcal{L}$ be the nonsymmetric Laplacian matrix associated with weighted directed graph $\mathcal{G}$. Then $\mathcal{L}$ has at least one zero eigenvalue and all its nonzero eigenvalues have positive real parts. Furthermore, $\mathcal{L}$ has a simple zero eigenvalue and all other eigenvalues have positive real parts if and only if $\mathcal{G}$ has a directed spanning tree. In addition, there exist $\mathbf{1}_n$, where $\mathbf{1}_n$ is the $n \times 1$ column vector of all ones, satisfying $\mathcal{L}\mathbf{1}_n = 0$ and $\mathbf{p} \in \mathbb{R}^n$ satisfying $\mathbf{p} \geq 0$, $\mathbf{p}^T\mathcal{L} = 0$, and $\mathbf{p}^T\mathbf{1}_n = 1$. [1]

Definition 3.1: Let μ_i, $i = 1, \ldots, n$, be the ith eigenvalue of $-\mathcal{L}$ with associated right eigenvector w_i and left eigenvector ν_i. Also let $\arg(\mu_i) = 0$ for $\mu_i = 0$ and $\arg(\mu_i) \in (\pi/2, 3\pi/2)$ for all $\mu_i \neq 0$, where $\arg(\cdot)$ denotes the phase of a number. Without loss of generality, suppose that μ_i is labeled such that $\arg(\mu_1) \leq \arg(\mu_2) \leq \cdots \leq \arg(\mu_n)$. [2]

Lemma 3.3: (see e.g., [19]) Given a rotation matrix $R \in \mathbb{R}^{3\times 3}$, let $\mathbf{a} = [a_1, a_2, a_3]^T$ and θ denote, respectively, the Euler axis (i.e., the unit vector in the direction of rotation) and Euler angle (i.e., the rotation angle). The eigenvalues of R are 1, $e^{\iota\theta}$, and $e^{-\iota\theta}$, where ι denotes the imaginary unit, with the associated right eigenvectors given by, respectively, $\varsigma_1 = \mathbf{a}$, $\varsigma_2 = [(a_2^2 + a_3^2)\sin^2(\theta/2), -a_1a_2\sin^2(\theta/2) + \iota a_3 \sin(\theta/2)|\sin(\theta/2)|, -a_1a_3\sin^2(\theta/2) - \iota a_2 \sin(\theta/2)|\sin(\theta/2)|]^T$, and $\varsigma_3 = \overline{\varsigma_2}$, where $\bar{\cdot}$ denotes the complex conjugate of a number. The associated left eigenvectors are, respectively, $\varpi_1 = \varsigma_1$, $\varpi_2 = \overline{\varsigma_2}$, and $\varpi_3 = \overline{\varsigma_3}$.

Lemma 3.4: Let $A \in \mathbb{R}^{n\times n}$ with eigenvalues γ_i and associated right and left eigenvectors q_i and s_i, respectively. Also let $B = \begin{bmatrix} 0_{n\times n} & I_n \\ A & -\alpha I_n \end{bmatrix}$, where $0_{n\times n}$ denotes the $n \times n$ zero matrix and α is a positive scalar. Then the eigenvalues of B are given by $\zeta_{2i-1} = (-\alpha + \sqrt{\alpha^2 + 4\gamma_i})/2$ with associated right and left eigenvectors $\begin{bmatrix} q_i \\ \zeta_{2i-1}q_i \end{bmatrix}$ and $\begin{bmatrix} (\zeta_{2i-1}+\alpha)s_i \\ s_i \end{bmatrix}$, respectively, and $\zeta_{2i} = (-\alpha - \sqrt{\alpha^2 + 4\gamma_i})/2$, with associated right and left eigenvectors $\begin{bmatrix} q_i \\ \zeta_{2i}q_i \end{bmatrix}$ and $\begin{bmatrix} (\zeta_{2i}+\alpha)s_i \\ s_i \end{bmatrix}$, respectively.

Proof: Suppose that ζ is an eigenvalue of B with an associated right eigenvector $\begin{bmatrix} f \\ g \end{bmatrix}$, where $f, g \in \mathbb{C}^n$. It follows that $\begin{bmatrix} 0_{n\times n} & I_n \\ A & -\alpha I_n \end{bmatrix}\begin{bmatrix} f \\ g \end{bmatrix} = \zeta \begin{bmatrix} f \\ g \end{bmatrix}$, which implies $g = \zeta f$ and $Af - \alpha g = \zeta g$. It thus follows that $Af = (\zeta^2 + \alpha\zeta)f$. Noting that $Aq_i = \gamma_i q_i$, we let $f = q_i$ and $\zeta^2 + \alpha\zeta = \gamma_i$. That is, each eigenvalue of A, γ_i, corresponds to two eigenvalues of B, denoted by $\zeta_{2i-1,2i} = (-\alpha \pm \sqrt{\alpha^2 + 4\gamma_i})/2$. Because $g = \zeta f$, it follows that the right eigenvectors associated with ζ_{2i-1} and ζ_{2i} are, respectively, $\begin{bmatrix} q_i \\ \zeta_{2i-1}q_i \end{bmatrix}$ and $\begin{bmatrix} q_i \\ \zeta_{2i}q_i \end{bmatrix}$. A similar analysis can be used to find the left eigenvectors of B associated with ζ_{2i-1} and ζ_{2i}. ■

Theorem 3.2: Suppose that weighted directed graph $\mathcal{G}$ has a directed spanning tree. Let the control algorithm for (1) be given by (3), where $r_i = [x_i, y_i, z_i]^T$ and $v_i = [v_{xi}, v_{yi}, v_{zi}]^T$. Let μ_i, w_i, ν_i, and $\arg(\mu_i)$ be defined in Definition 3.1, $\mathbf{p}$ be defined in Lemma 3.2, and $\mathbf{a} = [a_1, a_2, a_3]^T$, ς_k, and ϖ_k be defined in Lemma 3.3.

1) Suppose that $C = I_3$. Then all vehicles will eventually rendezvous if and only if $\alpha > \alpha^c$, where $\alpha^c \triangleq \max_i \sqrt{|\mu_i|\sin^2(\arg(\mu_i))/-\cos(\arg(\mu_i))}$. The rendezvous position is given by
$$\left[\mathbf{p}^T\left(x(0) + \frac{v_x(0)}{\alpha}\right), \mathbf{p}^T\left(y(0) + \frac{v_y(0)}{\alpha}\right), \mathbf{p}^T\left(z(0) + \frac{v_z(0)}{\alpha}\right)\right] \tag{4}$$
where x, y, z, v_x, v_y, and v_z are, respectively, column stack vectors of x_i, y_i, z_i, v_{xi}, v_{yi}, and v_{zi}.
2) Suppose that $C = R$, where R is the 3×3 rotation matrix defined in Lemma 3.3, and $\alpha > \alpha^c$. Given $|\mu_i|$, $i = 2, \ldots, n$, let $\psi_i^l \in (\pi/2, \pi)$ (respectively, $\psi_i^u \in (\pi, 3\pi/2)$) be the solution to $|\mu_i|\sin^2(\psi_i) + \alpha^2\cos(\psi_i) = 0$ if $\arg(\mu_i) \in (\pi/2, \pi]$ (respectively, $\arg(\mu_i) \in [\pi, 3\pi/2)$). If $|\theta| < \theta_d^c$, where $\theta_d^c \triangleq \min_{\arg(\mu_i)\in[\pi,3\pi/2)}(\psi_i^u - \arg(\mu_i))$, then all vehicles will eventually rendezvous at the position given by (4).
3) Under the assumption of 2), if $|\theta| = \theta_d^c$ and there exists a unique $\arg(\mu_\kappa) \in [\pi, 3\pi/2)$ such that $\psi_\kappa^u - \arg(\mu_\kappa) = \theta_d^c$, then all vehicles will eventually move on circular orbits with center given by (4) and period $\pi\alpha/|\mu_\kappa \sin(\psi_\kappa^u)|$. The radius of the orbit for vehicle i is given by $2|w_{\kappa(i)}p_c^T[r(0)^T, v(0)^T]^T|\sqrt{a_2^2 + a_3^2}\sin^2(\theta/2)$, where $w_{\kappa(i)}$ is the ith component of w_κ and $p_c = 1/(2\sigma_c + \alpha)\nu_\kappa^T w_\kappa \varpi_2^T \varsigma_2 \begin{bmatrix} (\sigma_c+\alpha)(\nu_\kappa \otimes \varpi_2) \\ \nu_\kappa \otimes \varpi_2 \end{bmatrix}$, where $\sigma_c = \iota(2|\mu_\kappa|\sin(\psi_\kappa^u)/\alpha)$. The relative radii of the orbits are equal to the relative magnitudes of $w_{\kappa(i)}$. The relative phases of the vehicles on their orbits are equal to the relative phases of $w_{\kappa(i)}$. The circular orbits are on a plane perpendicular to Euler axis $\mathbf{a}$.
4) Under the assumption of 2), if there exists a unique $\arg(\mu_\kappa) \in [\pi, 3\pi/2)$ such that $\psi_\kappa^u - \arg(\mu_\kappa) = \theta_d^c$ and $\theta_d^c < |\theta| < \min_{\arg(\mu_i)\in[\pi,3\pi/2), i\neq\kappa}(\psi_i^u - \arg(\mu_i))$, then the vehicles will eventually move along logarithmic spiral curves with center given by (4), growing rate $\mathrm{Re}(\sigma_s)$, where $\mathrm{Re}(\cdot)$ denotes the real part of a number and $\sigma_s = (-\alpha + \sqrt{\alpha^2 + 4\lambda_s})/2$ with $\lambda_s = \mu_\kappa e^{\iota|\theta|}$, and period $2\pi/|\mathrm{Im}(\sigma_s)|$, where $\mathrm{Im}(\cdot)$ represents the imaginary part

[1] That is, $\mathbf{1}_n$ and $\mathbf{p}$ are, respectively, the right and left eigenvectors of $\mathcal{L}$ associated with the zero eigenvalue.

[2] It follows from Lemma 3.2 that $\mu_1 = 0$, $w_1 = \mathbf{1}_n$, and $\nu_1 = \mathbf{p}$.

Authorized licensed use limited to: Utah State University. Downloaded on June 15, 2009 at 15:55 from IEEE Xplore. Restrictions apply.

of a number. The radius of the logarithmic spiral curve for vehicle i is $2|w_{\kappa(i)}p_s^T[r(0)^T, v(0)^T]^T e^{\mathrm{Re}(\sigma_s)t}\sqrt{a_2^2+a_3^2}\sin^2(\theta/2)$, where $p_s = 1/(2\sigma_s+\alpha)\nu_\kappa^T w_\kappa \varpi_2^T \varsigma_2 \left[\begin{smallmatrix}(\sigma_s+\alpha)(\nu_\kappa\otimes\varpi_2)\\ \nu_\kappa\otimes\varpi_2\end{smallmatrix}\right]$. The relative radii of the logarithmic spiral curves are equal to the relative magnitudes of $w_{\kappa(i)}$. The relative phases of the vehicles on their curves are equal to the relative phases of $w_{\kappa(i)}$. The curves are on a plane perpendicular to Euler axis $\mathbf{a}$.

Proof: 1) For the first statement, if $C = I_3$, then (1) using (3) can be written in matrix form as

$$\begin{bmatrix}\dot r\\ \dot v\end{bmatrix} = \left[\underbrace{\begin{bmatrix}0_{n\times n} & I_n\\ -\mathcal{L} & -\alpha I_n\end{bmatrix}}_{\Gamma}\otimes I_3\right]\begin{bmatrix} r\\ v\end{bmatrix} \tag{5}$$

where $r = [r_1^T,\ldots,r_n^T]^T$, $v = [v_1^T,\ldots,v_n^T]^T$, and $\mathcal{L}$ is the nonsymmetric Laplacian matrix associated with $\mathcal{G}$. It follows from the proof of Theorem 5.1 in [18] that the vehicles will eventually rendezvous if and only if Γ defined in (5) has a simple zero eigenvalue and all other eigenvalues have negative real parts. Note from Lemma 3.4 that each eigenvalue μ_i of $-\mathcal{L}$ corresponds to two eigenvalues of Γ given by $\zeta_{2i-1} = (-\alpha+\sqrt{\alpha^2+4\mu_i})/2$ with associated right and left eigenvectors $\left[\begin{smallmatrix} w_i\\ \zeta_{2i-1}w_i\end{smallmatrix}\right]$ and $\left[\begin{smallmatrix}(\zeta_{2i-1}+\alpha)\nu_i\\ \nu_i\end{smallmatrix}\right]$, respectively, and $\zeta_{2i} = (-\alpha-\sqrt{\alpha^2+4\mu_i})/2$, with associated right and left eigenvectors $\left[\begin{smallmatrix} w_i\\ \zeta_{2i}w_i\end{smallmatrix}\right]$ and $\left[\begin{smallmatrix}(\zeta_{2i}+\alpha)\nu_i\\ \nu_i\end{smallmatrix}\right]$, respectively, where $i = 1,\ldots,n$.

Because weighted directed graph $\mathcal{G}$ has a directed spanning tree, it follows from Lemma 3.2 that $-\mathcal{L}$ has a simple zero eigenvalue and all other eigenvalues have negative real parts. According to Definition 3.1, we let $\mu_1 = 0$ and $\mathrm{Re}(\mu_i) < 0$, $i = 2,\ldots,n$. Note from Lemma 3.2 that $w_1 = \mathbf{1}_n$ and $\nu_1 = \mathbf{p}$. It thus follows that $\zeta_1 = 0$ with associated right and left eigenvectors given by $\left[\begin{smallmatrix}\mathbf{1}_n\\ 0_n\end{smallmatrix}\right]$ and $\left[\begin{smallmatrix}\alpha\mathbf{p}\\ \mathbf{p}\end{smallmatrix}\right]$, respectively, and $\zeta_2 = -\alpha$. Note that $\zeta_2 < 0$ if $\alpha > 0$. Also noting that all $\sqrt{\alpha^2+4\mu_i}$ have nonnegative real parts, it follows that all ζ_{2i}, $i = 2,\ldots,n$, have negative real parts if $\alpha > 0$. It is left to show conditions under which ζ_{2i-1}, $i = 2,\ldots,n$, have negative real parts. Suppose that α_i^* is the critical value for α such that ζ_{2i-1}, $i = 2,\ldots,n$, is on the imaginary axis. Let $\zeta_{2i-1} = \eta_i\iota$, where $\eta_i\in\mathbb{R}$, $i = 2,\ldots,n$. After some manipulation, it follows that $\alpha_i^* = \sqrt{|\mu_i|\sin^2(\arg(\mu_i))/-\cos(\arg(\mu_i))}$ and $\eta_i = 2|\mu_i|\sin(\arg(\mu_i))/\alpha$, $i = 2,\ldots,n$. It is straightforward to verify that if $\alpha > \alpha_i^*$ (respectively, $\alpha < \alpha_i^*$), then ζ_{2i-1}, $i = 2,\ldots,n$, has a negative (respectively, positive) real part. Therefore, all ζ_{2i-1}, $i = 2,\ldots,n$, have negative real parts if and only if $\alpha > \max_{i=2,\ldots,n}\alpha_i^*$. Combining the above arguments shows that Γ has a simple zero eigenvalue and all other eigenvalues have negative real parts if and only if $\alpha > \alpha^c$.

Matrix Γ can be written in Jordan canonical form as SJS^{-1}, where the columns of S, denoted by s_k, $k = 1,\ldots,2n$, can be chosen to be the right eigenvectors or generalized right eigenvectors of Γ associated with eigenvalue ζ_k, $k = 1,\ldots,2n$, the rows of S^{-1}, denoted by h_k^T, $k = 1,\ldots,2n$, can be chosen to be the left eigenvectors or generalized left eigenvectors of Γ associated with eigenvalue ζ_k such that $h_k^T s_k = 1$ and $h_k^T s_\ell = 0$, $k\neq\ell$, and J is the Jordan block diagonal matrix with ζ_k being the diagonal entries. We can choose $s_1 = [\mathbf{1}_n^T, \mathbf{0}_n^T]^T$ and $h_1 = [\mathbf{p}^T, (1/\alpha)\mathbf{p}^T]^T$. It can be verified that $h_1^T s_1 = 1$. It thus follows that $\lim_{t\to\infty}\left[\begin{smallmatrix} r(t)\\ v(t)\end{smallmatrix}\right] = \lim_{t\to\infty}(e^{\Gamma t}\otimes I_3)\left[\begin{smallmatrix} r(0)\\ v(0)\end{smallmatrix}\right] = [(\left[\begin{smallmatrix}\mathbf{1}_n\\ \mathbf{0}_n\end{smallmatrix}\right][\mathbf{p}^T\ \ (1/\alpha)\mathbf{p}^T])\otimes I_3]\left[\begin{smallmatrix} r(0)\\ v(0)\end{smallmatrix}\right]$, which implies that $x_i(t)\to \mathbf{p}^T x(0)+(1/\alpha)\mathbf{p}^T v_x(0)$, $y_i(t)\to \mathbf{p}^T y(0)+(1/\alpha)\mathbf{p}^T v_y(0)$, $z_i(t)\to \mathbf{p}^T z(0)+(1/\alpha)\mathbf{p}^T v_z(0)$, $v_{xi}(t)\to 0$, $v_{yi}(t)\to 0$, and $v_{zi}(t)\to 0$ as $t\to\infty$. Equivalently, it follows that all vehicles will eventually rendezvous at the position given by (4).

2) For the second statement, using (3), (1) can be written in matrix form as

$$\begin{bmatrix}\dot r\\ \dot v\end{bmatrix} = \underbrace{\begin{bmatrix}0_{3n\times 3n} & I_{3n}\\ -(\mathcal{L}\otimes R) & -\alpha I_{3n}\end{bmatrix}}_{\Sigma}\begin{bmatrix} r\\ v\end{bmatrix}. \tag{6}$$

It follows from Lemmas 3.1 and 3.3 and Definition 3.1 that the eigenvalues of $-(\mathcal{L}\otimes R)$ are μ_i, $\mu_i e^{\iota\theta}$, and $\mu_i e^{-\iota\theta}$ with associated right eigenvectors $w_i\otimes\varsigma_1$, $w_i\otimes\varsigma_2$, and $w_i\otimes\varsigma_3$, respectively, and associated left eigenvectors $\nu_i\otimes\varpi_1$, $\nu_i\otimes\varpi_2$, and $\nu_i\otimes\varpi_3$, respectively. That is, the eigenvalues of $-(\mathcal{L}\otimes R)$ correspond to the eigenvalues of $-\mathcal{L}$ rotated by angles 0, θ, and $-\theta$, respectively. Let λ_ℓ, $\ell = 1,\ldots,3n$, denote the ℓth eigenvalue of $-(\mathcal{L}\otimes R)$. Without loss of generality, let $\lambda_{3i-2} = \mu_i$, $\lambda_{3i-1} = \mu_i e^{\iota\theta}$, and $\lambda_{3i} = \mu_i e^{-\iota\theta}$, $i = 1,\ldots,n$, be the eigenvalues of $-(\mathcal{L}\otimes R)$. Note from Lemma 3.4 that each λ_k corresponds to two eigenvalues of Σ, defined in (6), given by $\sigma_{2k-1,2k} = (-\alpha\pm\sqrt{\alpha^2+4\lambda_k})/2, k = 1,\ldots,3n$. Because $\mu_1 = 0$, it follows that $\lambda_1 = \lambda_2 = \lambda_3 = 0$, which in turn implies that $\sigma_1 = \sigma_3 = \sigma_5 = 0$ and $\sigma_2 = \sigma_4 = \sigma_6 = -\alpha$. Similar to the proof of the first statement, all σ_{2k}, $k = 1,\ldots,3n$, have negative real parts if $\alpha > 0$. Given $\alpha > 0$ and $\chi_i = |\mu_i|e^{\iota\arg(\chi_i)}$, $i = 2,\ldots,n$, ψ_i^l and ψ_i^u are the critical values for $\arg(\chi_i)\in[0,2\pi)$ such that $(-\alpha+\sqrt{\alpha^2+4\chi_i})/2$ is on the imaginary axis. In particular, if $\arg(\chi_i) = \psi_i^l$ (respectively, ψ_i^u), then $(-\alpha+\sqrt{\alpha^2+4\chi_i})/2 = \iota(2|\mu_i|\sin(\arg(\psi_i^l)/\alpha)$ (respectively, $\iota(2|\mu_i|\sin(\arg(\psi_i^u)/\alpha))$, $i = 2,\ldots,n$. If $\arg(\chi_i)\in(\psi_i^l,\psi_i^u)$ (respectively, $\arg(\chi_i)\in[0,\psi_i^l)\cup(\psi_i^u,2\pi)$), then $(-\alpha+\sqrt{\alpha^2+4\chi_i})/2$ have negative (respectively, positive) real parts. Because $\alpha > \alpha^c$, the first statement implies that all $(-\alpha+\sqrt{\alpha^2+4\mu_i})/2$, $i = 2,\ldots,n$, have negative real parts, which in turn implies that $\arg(\mu_i)\in(\psi_i^l,\psi_i^u)$, $i = 2,\ldots,n$. If $|\theta| < \theta_d^c$, then $\arg(\lambda_{3i-2})$, $\arg(\lambda_{3i-1})$, and $\arg(\lambda_{3i})$ are all within (ψ_i^l,ψ_i^u), which implies that σ_{6i-5}, σ_{6i-3}, and σ_{6i-1}, $i = 2,\ldots,n$, all have negative real parts. Therefore, if $|\theta| < \theta_d^c$, then Σ has exactly three zero eigenvalues and all other eigenvalues have negative real parts.

Similar to the proof of the first statement, we write Σ in Jordan canonical form as MJM^{-1}, where the columns of M, denoted by m_k, $k = 1,\ldots,6n$, can be chosen to be the right eigenvectors or generalized right eigenvectors of Σ associated with eigenvalue σ_k, the rows of M^{-1}, denoted by p_k^T, $k = 1,\ldots,6n$, can be chosen to be the left eigenvectors or generalized left eigenvectors of Σ associated with eigenvalue σ_k such that $p_k^T m_k = 1$ and $p_k^T m_\ell = 0$, $k\neq\ell$, and J is the Jordan block diagonal matrix with σ_k being the diagonal entries. Recall that the right and left eigenvectors of $-(\mathcal{L}\otimes R)$ associated with eigenvalue $\lambda_\ell = 0$ are, respectively, $\mathbf{1}_n\otimes\varsigma_\ell$ and $\mathbf{p}\otimes\varpi_\ell$, where $\ell = 1$, 2, 3. It in turn follows from Lemma 3.4 that the right and left eigenvectors of Σ associated with $\sigma_{2\ell-1} = 0$ are, respectively, $\left[\begin{smallmatrix}\mathbf{1}_n\otimes\varsigma_\ell\\ \mathbf{0}_{3n}\end{smallmatrix}\right]$ and $\left[\begin{smallmatrix}\alpha\mathbf{p}\otimes\varpi_\ell\\ \mathbf{p}\otimes\varpi_\ell\end{smallmatrix}\right]$, where $\ell = 1$, 2, 3. We can choose $m_{2\ell-1} = \left[\begin{smallmatrix}\mathbf{1}_n\otimes\varsigma_\ell\\ \mathbf{0}_{3n}\end{smallmatrix}\right]$ and $p_{2\ell-1} = \left[\begin{smallmatrix}\mathbf{p}\otimes(\varpi_\ell/\varpi_\ell^T\varsigma_\ell)\\ \mathbf{p}\otimes(\varpi_\ell/\alpha\varpi_\ell^T\varsigma_\ell)\end{smallmatrix}\right]$, where $\ell = 1$, 2, 3. It can be verified that $p_{2\ell-1}^T m_{2\ell-1} = 1$ and $p_{2\ell-1}^T m_{2k-1} = 0$, where $k,\ell = 1$, 2, 3 and $k\neq\ell$. Noting that $\sigma_{2\ell-1} = 0$, $\ell = 1$, 2, 3, it follows that $\lim_{t\to\infty}\left[\begin{smallmatrix} r(t)\\ v(t)\end{smallmatrix}\right] = \lim_{t\to\infty} M e^{Jt}M^{-1}\left[\begin{smallmatrix} r(0)\\ v(0)\end{smallmatrix}\right] \to (\sum_{\ell=1}^3 m_{2\ell-1}p_{2\ell-1}^T)\left[\begin{smallmatrix} r(0)\\ v(0)\end{smallmatrix}\right]$, which implies that $x_i(t)\to \mathbf{p}^T x(0)+(1/\alpha)\mathbf{p}^T v_x(0)$, $y_i(t)\to \mathbf{p}^T y(0)+(1/\alpha)\mathbf{p}^T v_y(0)$, $z_i(t)\to \mathbf{p}^T z(0)+(1/\alpha)\mathbf{p}^T v_z(0)$, $v_{xi}(t)\to 0$, $v_{yi}(t)\to 0$, and $v_{zi}(t)\to 0$ as $t\to\infty$. Equivalently, it follows that all vehicles will eventually rendezvous at the position given by (4).

3) For the third statement, if $\theta = \theta_d^c$ (respectively, $\theta = -\theta_d^c$) and there exists a unique $\arg(\mu_\kappa)\in[\pi,3\pi/2)$ such that $\psi_\kappa^u - \arg(\mu_\kappa) = \theta_d^c$, then $\lambda_{3\kappa-1} = \mu_\kappa e^{\iota\theta} = |\mu_\kappa|e^{\iota\psi_\kappa^u}$ (respectively, $\lambda_{3\kappa} = \mu_\kappa e^{-\iota\theta} = |\mu_\kappa|e^{\iota\psi_\kappa^u}$), which implies that $\sigma_{6\kappa-3} = (-\alpha+\sqrt{\alpha^2+4\lambda_{3\kappa-1}})/2 = \iota(2|\mu_\kappa|\sin(\psi_\kappa^u)/\alpha)$ (respectively, $\sigma_{6\kappa-1} = (-\alpha+\sqrt{\alpha^2+4\lambda_{3\kappa}})/2 = \iota(2|\mu_\kappa|\sin(\psi_\kappa^u)/\alpha)$). Noting that the complex eigenvalues of Σ are in pairs, it follows that Σ has an eigenvalue equal to $\overline{\sigma_{6\kappa-3}} = -\iota(2|\mu_\kappa|\sin(\psi_\kappa^u)/\alpha)$ (respectively, $\overline{\sigma_{6\kappa-1}} = -\iota(2|\mu_\kappa|\sin(\psi_\kappa^u)/\alpha)$), denoted by σ_* for simplicity. In this case, Σ has exactly three zero eigenvalues, two nonzero eigenvalues on the imaginary axis, and all other eigenvalues have negative real parts. In the following, we focus on $\theta = \theta_d^c$ since the analysis for $\theta = -\theta_d^c$ is similar except that all vehicles will move in reverse directions. Note from Lemma 3.4 that the right and left eigenvectors associated with $\sigma_{6\kappa-3}$ are, respectively, $\left[\begin{smallmatrix} w_\kappa\otimes\varsigma_2\\ \sigma_{6\kappa-3}(w_\kappa\otimes\varsigma_2)\end{smallmatrix}\right]$ and

Authorized licensed use limited to: Utah State University. Downloaded on June 15, 2009 at 15:55 from IEEE Xplore. Restrictions apply.

$\begin{bmatrix}(\sigma_{6\kappa-3}+\alpha)(\nu_\kappa\otimes\varpi_2)\\ \nu_\kappa\otimes\varpi_2\end{bmatrix}$. We can choose $m_{6\kappa-3}=\begin{bmatrix}w_\kappa\otimes\varsigma_2\\ \sigma_{6\kappa-3}(w_\kappa\otimes\varsigma_2)\end{bmatrix}$ and $p_{6\kappa-3}=(1/(2\sigma_{6\kappa-3}+\alpha)\nu_\kappa^T w_\kappa \varpi_2^T\varsigma_2)\begin{bmatrix}(\sigma_{6\kappa-3}+\alpha)(\nu_\kappa\otimes\varpi_2)\\ \nu_\kappa\otimes\varpi_2\end{bmatrix}$. It can be verified that $p_{6\kappa-3}^T m_{6\kappa-3}=1$. Similarly, it follows that m_* and p_* corresponds to σ_* are given by $m_*=\overline{m_{6\kappa-3}}$ and $p_*=\overline{p_{6\kappa-3}}$. It follows that $\begin{bmatrix}r(t)\\ v(t)\end{bmatrix}=e^{\Sigma t}\begin{bmatrix}r(0)\\ v(0)\end{bmatrix}\to(\sum_{\ell=1}^3 m_{2\ell-1}p_{2\ell-1}^T)\begin{bmatrix}r(0)\\ v(0)\end{bmatrix}+c(t)$ for large t, where $c(t)\triangleq(e^{\iota(2|\mu_\kappa|\sin(\psi_\kappa^u)/\alpha)t}m_{6\kappa-3}p_{6\kappa-3}^T+e^{-\iota(2|\mu_\kappa|\sin(\psi_\kappa^u)/\alpha)}m_*p_*^T)\begin{bmatrix}r(0)\\ v(0)\end{bmatrix}$. Let $c_k(t)$ be the kth component of $c(t)$, $k=1,\ldots,6n$. It follows that $c_{3(i-1)+\ell}(t)=2\mathrm{Re}(e^{\iota(2|\mu_\kappa|\sin(\psi_\kappa^u)/\alpha)t}w_{\kappa(i)}\varsigma_{2(\ell)}p_{6\kappa-3}^T\ [r(0)^T,v(0)^T]^T)$, where $i=1,\ldots,n$, $\ell=1,2,3$, and $\varsigma_{2(\ell)}$ denotes the ℓth component of ς_2. After some manipulation, it follows that $c_{3(i-1)+\ell}(t)=2|\varsigma_{2(\ell)}w_{\kappa(i)}p_{6\kappa-3}^T[r(0)^T,v(0)^T]^T|\cos((2|\mu_\kappa|\sin(\psi_\kappa^u)/\alpha)t+\arg(w_{\kappa(i)}p_{6\kappa-3}^T[r(0)^T,v(0)^T]^T)+\arg(\varsigma_{2(\ell)}))$, $i=1,\ldots,n$, $\ell=1,2,3$. Therefore, it follows that $x_i(t)\to\mathbf{p}^Tx(0)+(1/\alpha)\mathbf{p}^Tv_x(0)+c_{3i-2}(t)$, $y_i(t)\to\mathbf{p}^Ty(0)+(1/\alpha)\mathbf{p}^Tv_y(0)+c_{3i-1}(t)$, and $z_i(t)\to\mathbf{p}^Tz(0)+(1/\alpha)\mathbf{p}^Tv_z(0)+c_{3i}(t)$ for large t. After some manipulation, it can be verified that $\|[c_{3i-2}(t),c_{3i-1}(t),c_{3i}(t)]^T\|=2|w_{\kappa(i)}p_{6\kappa-3}^T[r(0)^T,v(0)^T]^T|\sqrt{a_2^2+a_3^2}\sin^2(\theta/2)$, which is a constant. Therefore, it follows that all vehicles will eventually move on circular orbits with center give by (4) and period $\pi\alpha/|\mu_\kappa\sin(\psi_\kappa^u)|$. The radius of the orbit for vehicle i is given by $2|w_{\kappa(i)}p_{6\kappa-3}^T[r(0)^T,v(0)^T]^T|\sqrt{a_2^2+a_3^2}\sin^2(\theta/2)$. The relative radii of the orbits are equal to the relative magnitudes of $w_{\kappa(i)}$. In addition, the relative phases of the vehicles are equal to the relative phases of $w_{\kappa(i)}$. Note from Lemma 3.3 that Euler axis $\mathbf{a}$ is orthogonal to both $\mathrm{Re}(\varsigma_2)$ and $\mathrm{Im}(\varsigma_2)$ are applied componentwise. It can thus be verified that $\mathbf{a}$ is orthogonal to $[c_{3i-2}(t),c_{3i-1}(t),c_{3i}(t)]^T$, which implies that the circular orbits are on a plane perpendicular to $\mathbf{a}$.

4) For the fourth statement, if there exists a unique $\arg(\mu_\kappa)\in[\pi,3\pi/2)$ such that $\psi_\kappa^u-\arg(\mu_\kappa)=\theta_d^c$ and $\theta_d^c<\theta<\min_{\arg(\mu_i)\in[\pi,3\pi/2),i\neq\kappa}(\psi_i^u-\arg(\mu_i))$ (respectively, $-\min_{\arg(\mu_i)\in[\pi,3\pi/2),i\neq\kappa}(\psi_i^u-\arg(\mu_i))<\theta<-\theta_d^c$), then $\lambda_{3\kappa-1}=\mu_\kappa e^{\iota\theta}=|\mu_\kappa|e^{\iota(\arg(\mu_\kappa)+\theta)}$ (respectively, $\lambda_{3\kappa}=\mu_\kappa e^{-\iota\theta}=|\mu_\kappa|e^{\iota(\arg(\mu_\kappa)-\theta)}$), where $\arg(\mu_\kappa)+\theta>\psi_\kappa^u$ (respectively, $\arg(\mu_\kappa)-\theta>\psi_\kappa^u$), which implies that $\sigma_{6\kappa-3}=(-\alpha+\sqrt{\alpha^2+4\lambda_{3\kappa-1}})/2$ (respectively, $\sigma_{6\kappa-1}=(-\alpha+\sqrt{\alpha^2+4\lambda_{3\kappa}})/2$) has a positive real part. A similar argument as above shows that Σ has exactly three zero eigenvalues and two eigenvalues with positive real parts and all other eigenvalues have negative real parts. By following a similar procedure to the proof of the third statement, we can show that all vehicles will eventually move along logarithmic spiral curves with center given by (4), growing rate $\mathrm{Re}(\sigma_{6\kappa-3})$, and period $2\pi/|\mathrm{Im}(\sigma_{6\kappa-3})|$. The radius of the logarithmic spiral curve for vehicle i is given by $2|w_{\kappa(i)}p_{6\kappa-3}^T[r(0)^T,v(0)^T]^T|e^{\mathrm{Re}(\sigma_{6\kappa-3})t}\sqrt{a_2^2+a_3^2}\sin^2(\theta/2)$. The relative radii of the logarithmic spiral curves are equal to the relative magnitudes of $w_{\kappa(i)}$. In addition, the relative phases of the vehicles on their curves are equal to the relative phases of $w_{\kappa(i)}$. A similar argument to that for the third statement shows that the curves are on a plane perpendicular to Euler axis $\mathbf{a}$. ■

Example 3.3: To illustrate, consider four vehicles with network topology $\mathcal{G}$ shown by Fig. 1. Let $\mathcal{L}$ associated with $\mathcal{G}$ be given by

$$\begin{bmatrix}1.5 & 0 & -1.1 & -0.4\\ -1.2 & 1.2 & 0 & 0\\ -0.1 & -0.5 & 0.6 & 0\\ -1 & 0 & 0 & 1\end{bmatrix}.$$

It can be computed that $\theta_d^c=0.3557$ rad. Let R be the rotation matrix corresponding to Euler axis $\mathbf{a}=(1/14)[1,2,3]^T$ and Euler angle $\theta=\theta_d^c$. It can also be computed that $\alpha^c=0.3626$. We let $\alpha=\alpha^c+0.5$. Fig. 2 shows the eigenvalues of $-\mathcal{L}$ and $-(\mathcal{L}\otimes R)$. We can see that the eigenvalues of $-(\mathcal{L}\otimes R)$ correspond to the eigenvalues of $-\mathcal{L}$ rotated by angles 0, θ, and $-\theta$. Fig. 3 shows the eigenvalues of Σ.

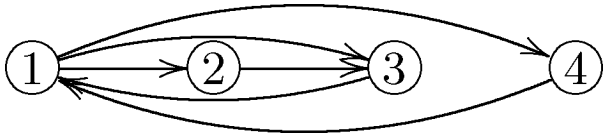

Fig. 1. Network topology for four vehicles. An arrow from j to i denotes that vehicle i can receive information from vehicle j.

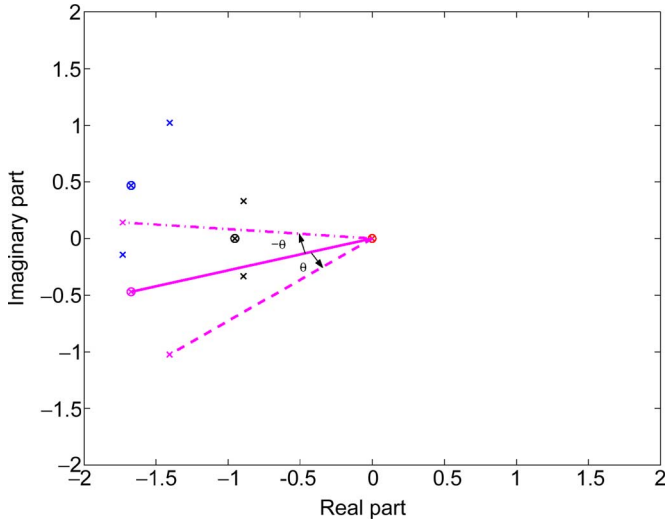

Fig. 2. Eigenvalues of $-\mathcal{L}$ and $-(\mathcal{L}\otimes R)$ with $\theta=\theta_d^c$. Circles denote the eigenvalues of $-\mathcal{L}$ while x-marks denote the eigenvalues of $-(\mathcal{L}\otimes R)$. The eigenvalues of $-(\mathcal{L}\otimes R)$ correspond to the eigenvalues of $-\mathcal{L}$ rotated by angles $0,\theta$, and $-\theta$, respectively. In particular, the eigenvalues obtained by rotating μ_4 by angles $0,\theta$, and $-\theta$ are shown by, respectively, the solid line, the dashed line, and the dashdot line.

We can see that each eigenvalue of $-(\mathcal{L}\otimes R)$, λ_k, corresponds to two eigenvalues of Σ, $\sigma_{2k-1,2k}$, where $\sigma_{2k-1,2k}=(-\alpha\pm\sqrt{\alpha^2+4\lambda_k})/2$, $k=1,\ldots,12$. Because $\theta=\theta_d^c$ and $\alpha>\alpha^c$, two nonzero eigenvalues of Σ are located on the imaginary axis as shown in Fig. 2.

B. Discussion and Extension

In this subsection, we discuss the results in Section III-A and show an extension to single-integrator kinematics. In existing consensus algorithms for double-integrator dynamics (e.g., [9], [18]), the Cartesian coordinates of a vehicle are decoupled. We have shown in Theorem 3.2 that different collective motions can result from the Cartesian coordinate coupling. In addition, the first statement of Theorem 3.2 generalizes Theorem 5.1 in [18], which gives only a sufficient condition for α, by giving a necessary and sufficient condition.

The results in Section III-A extend [13] threefold, namely, extension from 2-D to 3-D, extension from single-integrator kinematics to double-integrator dynamics without the knowledge of relative velocities, and extension from a unidirectional ring topology to a general network topology. While [13] proposes an extension from single-integrator kinematics to double-integrator dynamics to deal with a formation control problem, the extension relies not only on relative positions but also on relative velocities between neighbors. In contrast, algorithm (3) does not rely on relative velocities between neighbors. For vehicles with nonholonomic constraints, algorithm (3) can still be applied if the vehicle dynamics can be feedback linearized as double-integrator dynamics.

For single-integrator kinematics given by

$$\dot{r}_i=u_i,\quad i=1,\ldots,n \tag{7}$$

Authorized licensed use limited to: Utah State University. Downloaded on June 15, 2009 at 15:55 from IEEE Xplore. Restrictions apply.

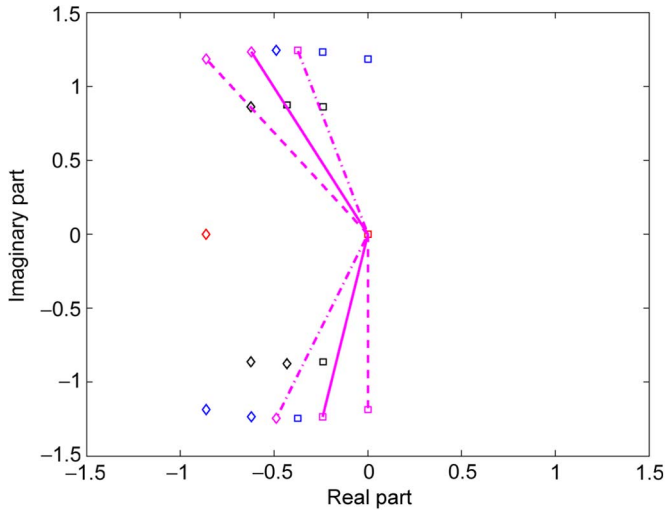

Fig. 3. Eigenvalues of Σ. Squares denote the eigenvalues computed by $\sigma_{2k-1} = (-\alpha + \sqrt{\alpha^2 + 4\lambda_k})/2$ while diamonds denote the eigenvalues computed by $\sigma_{2k} = (-\alpha - \sqrt{\alpha^2 + 4\lambda_k})/2, k = 1, \ldots, 12$. In particular, the eigenvalues of Σ correspond to $\lambda_{10} = \mu_4$, $\lambda_{11} = \mu_4 e^{\iota\theta}$, and $\lambda_{12} = \mu_4 e^{-\iota\theta}$ are shown by, respectively, the solid line, the dashed line, and the dashdot line. Because $\theta = \theta_d^c$, two nonzero eigenvalues of Σ are on the imaginary axis.

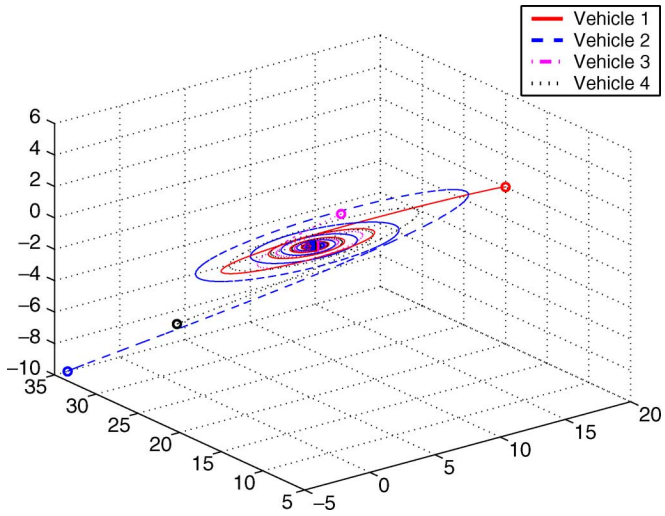

Fig. 4. Trajectories of the four vehicles using (3) with $\theta = \theta_d^c - 0.2$. Circles denote the starting positions of the vehicles while the squares denote the snapshots of the vehicles at $t = 30$.

where $r_i = [x_i, y_i, z_i]^T$ is the position and $u_i \in \mathbb{R}^3$ is the control input associated with the ith vehicle, a consensus algorithm with Cartesian coordinate coupling takes in the form

$$u_i = -\sum_{j=1}^{n} a_{ij} R(r_i - r_j), \quad i = 1, \ldots, n \tag{8}$$

where R is the 3×3 rotation matrix. We can adopt a similar approach to that used in Theorem 3.2 to analyze (8). Due to space limitation, we present the following theorem with its proof omitted.

Theorem 3.4: Suppose that weighted directed graph $\mathcal{G}$ has a directed spanning tree. Let the control algorithm for (7) be given by (8). Let μ_i, w_i, ν_i, and $\arg(\mu_i)$ be defined in Definition 3.1, $\mathbf{p}$ be defined in Lemma 3.2, and $\mathbf{a} = [a_1, a_2, a_3]^T$, ς_k, and ϖ_k be defined in Lemma 3.3.

1) If $|\theta| < \theta_s^c$, where $\theta_s^c \triangleq (3\pi/2) - \arg(\mu_n)$, the vehicles will eventually rendezvous at position $(\mathbf{p}^T x, \mathbf{p}^T y, \mathbf{p}^T z)$, where x, y, and z are, respectively, column stack vectors of x_i, y_i, and z_i.
2) If $|\theta| = \theta_s^c$ and $\arg(\mu_n)$ is the unique maximum phase of μ_i, all vehicles will eventually move on circular orbits with center $(\mathbf{p}^T x, \mathbf{p}^T y, \mathbf{p}^T z)$ and period $2\pi/|\mu_n|$. The radius of the orbit for vehicle i is given by $2|w_{n(i)}(\nu_n^T/\nu_n^T w_n \otimes \varpi_2^T/\varpi_2^T \varsigma_2) r(0)| \sqrt{a_2^2 + a_3^2}\, \sin^2(\theta/2)$, where $w_{n(i)}$ is the ith component of w_n. The relative radii of the orbits are equal to the relative magnitudes of $w_{n(i)}$. The relative phases of the vehicles on their orbits are equal to the relative phases of $w_{n(i)}$. The circular orbits are on a plane perpendicular to Euler axis $\mathbf{a}$.
3) If $\arg(\mu_n)$ is the unique maximum phase of μ_i and $\theta_s^c < |\theta| < (3\pi/2) - \arg(\mu_{n-1})$, all vehicles will eventually move along logarithmic spiral curves with center $(\mathbf{p}^T x, \mathbf{p}^T y, \mathbf{p}^T z)$, growing rate $|\mu_n| \cos(\arg(\mu_n) + |\theta|)$, and period $2\pi/(|\mu_n \sin(\arg(\mu_n) + |\theta|)|)$. The radius of the logarithmic spiral curve for vehicle i is given by $2|w_{n(i)}(\nu_n^T/\nu_n^T w_n \otimes \varpi_2^T/\varpi_2^T \varsigma_2) r(0)|$ $e^{[|\mu_n| \cos(\arg(\mu_n) + |\theta|)]t} \sqrt{a_2^2 + a_3^2} \sin^2(\theta/2)$. The relative radii of the logarithmic spiral curves are equal to the relative magnitudes of $w_{n(i)}$. The relative phases of the vehicles on their curves are equal to the relative phases of $w_{n(i)}$. The logarithmic spiral curves are on a plane perpendicular to Euler axis $\mathbf{a}$.

Corollary 3.5: Suppose that weighted directed graph $\mathcal{G}$ is a unidirectional ring (i.e., a cyclic pursuit topology). Also suppose that $a_{ij} = 1$ if $(j, i) \in \mathcal{E}$ and $a_{ij} = 0$ otherwise. Let the control algorithm for (7) be given by (8), where $r_i = [x_i, y_i]^T$ and R is the 2×2 rotation matrix given by $R(\theta) = \begin{bmatrix} \cos(\theta) & \sin(\theta) \\ -\sin(\theta) & \cos(\theta) \end{bmatrix}$.

1) If $|\theta| < (\pi/n)$, the vehicles will eventually rendezvous at position $(\mathbf{p}^T x, \mathbf{p}^T y)$, where $x = [x_1, \ldots, x_n]^T$ and $y = [y_1, \ldots, y_n]^T$.
2) If $|\theta| = \pi/n$, all vehicles will eventually move on the same circular orbit with center $(\mathbf{p}^T x, \mathbf{p}^T y)$, period $\pi/(\sin(\pi/n))$, and radius $2|w_{n(i)}(\nu_n^T/\nu_n^T w_n \otimes [1/2, -(1/2)\iota]) r(0)|$.[3] In addition, the vehicles will eventually be evenly distributed on the orbit.
3) If $(\pi/n) < |\theta| < (2\pi/n)$, all vehicles will eventually move along logarithmic spiral curves with center $(\mathbf{p}^T x, \mathbf{p}^T y)$, growing rate $2 \sin(\pi/n) \sin(|\theta| - (\pi/n))$, period $\pi/\sin(\pi/n) \cos(|\theta| - \pi/n)$, and radius $2|w_{n(i)}((\nu_n^T/\nu_n^T w_n) \otimes [1/2, -(1/2)\iota]) r(0)|$ $e^{2 \sin(\pi/n) \sin(|\theta| - (\pi/n))t}$. In addition, the phases of all vehicles will eventually be evenly distributed.

Proof: Note that if weighted directed graph $\mathcal{G}$ is a unidirectional ring and $a_{ij} = 1$ if $(j, i) \in \mathcal{E}$ and $a_{ij} = 0$ otherwise, then $\mathcal{L}$ is a circulant matrix. Also note that a circulant matrix can be diagonalized by a Fourier matrix. The proof then follows Theorem 3.4 directly by use of the properties of the eigenvalues of a circulant matrix and the properties of the Fourier matrix. ■

Corollary 3.5 was proved in [13] by use of parametric spectral analysis of some special types of circulant matrices. Here we have shown that the convergence result in [13] is a special case of Theorem 3.4 and can be recovered by exploiting the properties of the circulant matrices and the Kronecker product. When $\mathcal{G}$ is a unidirectional ring but different positive weights are chosen for a_{ij}, where $(j, i) \in \mathcal{E}$, all vehicles will move on orbits with different radii and their phases will not be evenly distributed.

IV. Simulation

In this section, we study collective motions of four vehicles using (3). Suppose that the network topology is given by Fig. 1 and $\mathcal{L}$ is defined in Example 3.3. Let θ_d^c, $\mathbf{a}$, and α be given in Example 3.3. It can be verified that there exists a unique $\arg(\mu_4) \in [\pi, 3\pi/2)$ such that $\psi_4^u - \arg(\mu_4) = \theta_d^c$ (i.e., $\kappa = 4$ in Theorem 3.2). It can also be computed that the right eigenvector of $-\mathcal{L}$ associated with eigenvalue μ_4 is $w_4 = [-0.2847 - 0.2820\iota, 0.7213, -0.2501 + 0.1355\iota, 0.4809 + 0.0837\iota]^T$ and $\mathbf{p} = [0.2502, 0.1911, 0.4587, 0.1001]^T$.

Figs. 4, 5, and 6 show, respectively, the trajectories of the four vehicles using (3) with $\theta = \theta_d^c - 0.2$, $\theta = \theta_d^c$, and $\theta = \theta_d^c + 0.2$. It can

[3]In this case, all $w_{n(i)}$, $i = 1, \ldots, n$, have the same magnitude.

Authorized licensed use limited to: Utah State University. Downloaded on June 15, 2009 at 15:55 from IEEE Xplore. Restrictions apply.

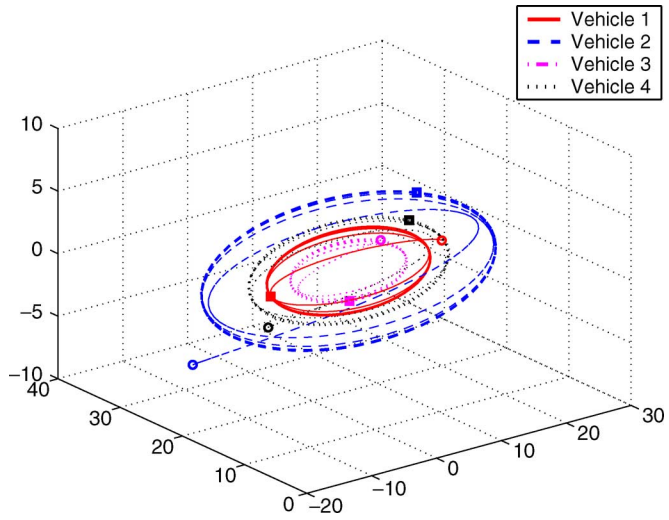

Fig. 5. Trajectories of the four vehicles using (3) with $\theta = \theta_d^c$. Circles denote the starting positions of the vehicles while the squares denote the snapshots of the vehicles at $t = 30$.

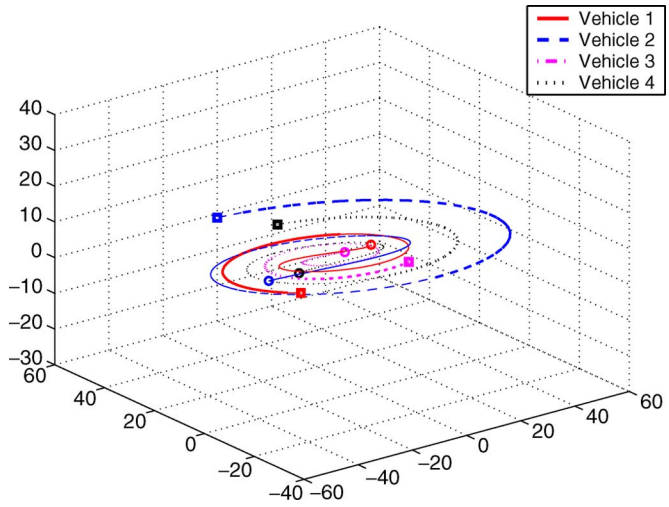

Fig. 6. Trajectories of the four vehicles using (3) with $\theta = \theta_d^c + 0.2$. Circles denote the starting positions of the vehicles while the squares denote the snapshots of the vehicles at $t = 10$.

be seen that all vehicles eventually rendezvous at the position given by (4) when $\theta = \theta_d^c - 0.2$, move on circular orbits when $\theta = \theta_d^c$, and move along logarithmic spiral curves when $\theta = \theta_d^c + 0.2$. Also observe that when $\theta = \theta_d^c$, the relative radii of the circular orbits (respectively, the relative phases of the vehicles) are equal to the relative magnitudes (respectively, phases) of the components of w_4. In addition, the trajectories of all vehicles are perpendicular to Euler axis $\mathbf{a}$ in all cases. A similar pattern for the relative radii and phases can also be observed for the logarithmic spiral curves.

V. Conclusion

We have introduced Cartesian coordinate coupling to a consensus algorithm for double-integrator dynamics by a rotation matrix in 3-D. We have shown conditions under which rendezvous, circular patterns, and logarithmic spiral patterns can be achieved using the algorithm with Cartesian coordinate coupling under a general network topology and quantitatively characterize the resulting collective motions. We have also demonstrated collective motions of four vehicles using the introduced algorithm in simulation. In future work, we will apply the algorithm in experiments in motion coordination of robotic networks. The robustness of the case of circular orbits can be improved by letting the Euler angle vary slightly below or above its critical value rather than remain constant at its critical value in case that the resulting trajectories spiral out or spiral in. We will also study a synthesis problem, namely, how to design the network topology such that some trajectories with desired relative radii and relative phases can be achieved.

References

[1] A. Jadbabaie, J. Lin, and A. S. Morse, "Coordination of groups of mobile autonomous agents using nearest neighbor rules," *IEEE Trans. Automat. Control*, vol. 48, no. 6, pp. 988–1001, Jun. 2003.

[2] R. Olfati-Saber, J. A. Fax, and R. M. Murray, "Consensus and cooperation in networked multi-agent systems," *Proc. IEEE*, vol. 95, no. 1, pp. 215–233, Jan. 2007.

[3] W. Ren, R. W. Beard, and E. M. Atkins, "Information consensus in multivehicle cooperative control," *IEEE Control Syst. Mag.*, vol. 27, no. 2, pp. 71–82, 2007.

[4] G. Lafferriere, A. Williams, J. Caughman, and J. J. P. Veerman, "Decentralized control of vehicle formations," *Syst. Control Lett.*, vol. 54, no. 9, pp. 899–910, 2005.

[5] R. Olfati-Saber, "Flocking for multi-agent dynamic systems: Algorithms and theory," *IEEE Trans. Automati. Control*, vol. 51, no. 3, pp. 401–420, Mar. 2006.

[6] W. Ren and E. M. Atkins, "Distributed multi-vehicle coordinated control via local information exchange," *Int. J. Robust Nonlin. Control*, vol. 17, no. 10–11, pp. 1002–1033, 2007.

[7] D. Lee and M. W. Spong, "Stable flocking of multiple inertial agents on balanced graphs," *IEEE Trans. Automat. Control*, vol. 52, no. 8, pp. 1469–1475, Aug. 2007.

[8] H. G. Tanner, A. Jadbabaie, and G. J. Pappas, "Flocking in fixed and switching networks," *IEEE Trans. Automat. Control*, vol. 52, no. 5, pp. 863–868, May 2007.

[9] G. Xie and L. Wang, "Consensus control for a class of networks of dynamic agents," *Int. J. Robust Nonlin. Control*, vol. 17, no. 10–11, pp. 941–959, 2007.

[10] Z. Lin, M. Broucke, and B. Francis, "Local control strategies for groups of mobile autonomous agents," *IEEE Trans. Automat. Control*, vol. 49, no. 4, pp. 622–629, Apr. 2004.

[11] A. Sinha and D. Ghose, "Generalization of linear cyclic pursuit with application to rendezvous of multiple autonomous agents," *IEEE Trans. Automat. Control*, vol. 51, no. 11, pp. 1819–1824, Nov. 2006.

[12] J. A. Marshall, M. E. Broucke, and B. A. Francis, "Pursuit formations of unicycles," *Automatica*, vol. 42, no. 1, pp. 3–12, 2006.

[13] M. Pavone and E. Frazzoli, "Decentralized policies for geometric pattern formation and path coverage," *ASME J. Dyn. Syst., Meas., Control*, vol. 129, no. 5, pp. 633–643, 2007.

[14] E. W. Justh and P. S. Krishnaprasad, "Equilibria and steering laws for planar formations," *Syst. Control Lett.*, vol. 52, pp. 25–38, 2004.

[15] D. A. Paley, N. E. Leonard, R. Sepulchre, D. Grünbaum, and J. K. Parrish, "Oscillator models and collective motion," *IEEE Control Syst. Mag.*, vol. 27, no. 4, pp. 89–105, 2007.

[16] W. Ren, "Collective motion from consensus with Cartesian coordinate coupling—Part i: Single-integrator kinematics & part ii: Double-integrator dynamics," in *Proc. IEEE Conf. Decision Control*, Cancun, Mexico, Dec. 2008, pp. 1006–1017.

[17] R. Agaev and P. Chebotarev, "On the spectra of nonsymmetric Laplacian matrices," *Linear Algebra Appl.*, vol. 399, pp. 157–178, 2005.

[18] W. Ren, "On consensus algorithms for double-integrator dynamics," *IEEE Trans. Automat. Control*, vol. 53, no. 6, pp. 1503–1509, Jul. 2008.

[19] [Online]. Available: http://www.mathpages.com/home/kmath593/kmath593.htm

Authorized licensed use limited to: Utah State University. Downloaded on June 15, 2009 at 15:55 from IEEE Xplore. Restrictions apply.